International Journal of advancement in electronics and computer engineering (IJAECE)
Volume 3, Issue 4, July 2014, pp.317-323, ISSN 2278 -1412

New Raman Spectrometer of CSIR-NPL for the Advanced Characterization of the Novel Materials

Sugandha Dogra Pandey[1], K. Samanta[2], Jasveer Singh[3], Nita Dilawar Sharma[4] , A. K. Bandyopadhyay[5]

[1,2,3,4,5]*Vacuum & Pressure Standards, National Physical Laboratory, New Delhi, akband@nplindia.org,India;*

Abstract *– A new Raman spectrometer with options to go down to low temperatures of 4.2 K and high pressure up to 20 GPa has been installed recently. The spectrometer was calibrated using various standard reference materials e.g. silicon, diamond and Ge etc. A large number of samples both at room temperature and at low temperatures have been studied. We shall be reporting here Raman Spectroscopic studies of five technologically novel materials at room temperature namely GaN, Cu_2ZnSnS_4 (CZTS), Doped Lithium Niobate ($LiNbO_3$), YVO_4 [Eu^{+3}, Sm^{+3}] and finally Sb_2Te_3. For low temperature studies, we have selected Sb_2Te_3 up to 77 K. We have analyzed the results from the theoretical estimation of optical phonons which are described by the irreducible representation of the crystal structures and then compared these with the experimental data. For low temperature studies, the temperature dependent Raman frequency shift has been studied. The systematic shifts have been explained in light of the thermal expansion and anharmonic phonon-phonon interactions. In both these studies [room & low temperatures], close agreements between the theoretically obtained data with the experimentally obtained Raman modes or shift are very encouraging.*

I. Introduction

Raman spectroscopy has proved to be an invaluable, powerful and widely used non destructive optical method for investigating the dynamics of different states of matter. The beauty of this method is that it provides distinctive features or Raman active modes which are useful for the characterization of most materials. With fast advancement in technology, the incorporation of multiple grating monochromators with charged coupled device (CCD) arrangement etc. have led to tremendous improvement in the obtained Raman spectra by providing higher resolving powers with increase in quantum efficiency and very low dark count rates resulting in increase in sensitivity. Thus Raman spectroscopy is a very useful tool and it is now widely used for identification of the structure, bonding, phase transitions etc.

Since 1992, our group at NPLI, has been actively working in the field of Raman spectroscopy with studies of materials under high pressure using a single stage Jobin Yvon-Spex monochromator (HR 640) with a notch filter to suppress the Rayleigh line [1]. A series of samples have been studied [2-4] and also some theoretical studies carried out [5]. However in 2012, the group has acquired a High Resolution Raman Spectrometer [Horiba Jobin-Yvon, France, modelT64000] under a CSIR project "Advances in strology- NWP-45". This Raman Spectrometer is a three stage monochromator (Triple Monochromator) with optics, aperture and coupling optimized for performance. The capability and performance are very unique - the focal length is 640 mm (single stage) and thus 3 x 640 mm (triple additive), Step size: 0.00066 nm (with 1800 gr/mm gratings) and low frequency: typically 5 cm^{-1}, reproducibility: better than 1 pixel, stray light rejection: 10^{-14} at 20 cm^{-1} (514 nm laser). As a result of these stringent specifications, the spectrometer works from ultra-low frequency measurements $\geq$5cm^{-1} with very high spectral resolution down to 0.15 cm^{-1}. As the stability of data of this integrated triple spectrometer is very high, first- and second-order Raman spectra even with low frequency close to Rayleigh line can be obtained easily.

A 5 watt Argon ion laser, model Stabilite 2017 from Spectra-physics Inc., USA with selected wavelength of 514.5 nm is used as the source of excitation. Usually, laser power on sample is kept at about 80mW – 100mW. The Raman signal is detected using CCD which is connected to the output port of the monochromator. The obtained Raman spectrum is usually deconvoluted using Voigt fit. The spectrometer has the provisions to carry out studies at low temperature down to 4.2 K and high pressure up to 20 GPa. A continuous flow cryostat was used for attaining low temperatures down to 4.2 K with a PID temperature controller for controlling the temperature. The fluid is pumped from a dewar with the help of a stainless steel transfer line. The sample is mounted in a vacuum sealed chamber where a base

vacuum of the order of 10^{-6} torr is attained with a turbo molecular pump. The cryostat has the provision to go to a high temperature up to 450 K. The cryostat can be used for liquid nitrogen with suitable modification.During the period of slightly less than one year, manygroups have been provided the Raman analysis of the samples. The present report is a brief description of the results obtained with these samples.

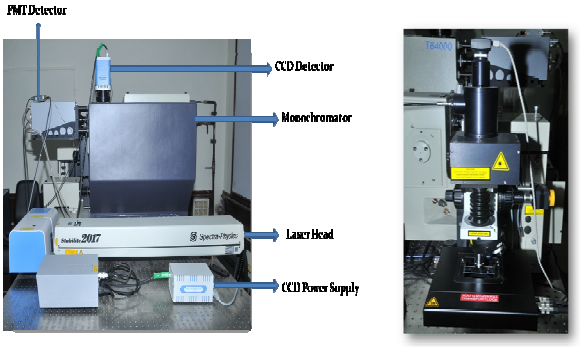

Fig. 1. Triple Raman Spectrometer with microscope used for present studies

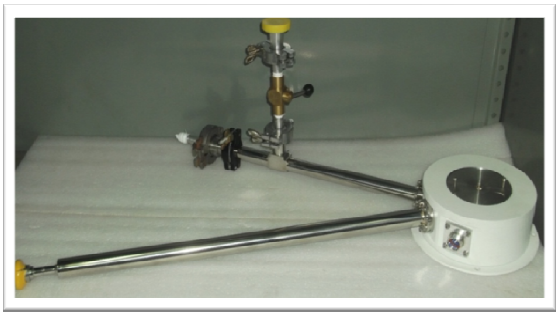

Fig. 2. Liquid Nitrogen/He cryostat.

Calibrations of the TR64000 Spectrometer:The spectrometer is calibrated using standard samples of Si, Ge, GaAs etc. Figure 3 shows the Raman Shift of these two samples. The agreement between the present value with the reported one is excellent.

Two types of experiments were carried out – (1) Raman Spectra taken at Room Temperature and (2) Raman Spectra taken at variable Temperature.

1) Room Temperature studies:

A) GaN layers were grown on Sapphire substrate (001) using Ga target with different growth temperatures 300-600 ^{o}C by Laser MBE technique

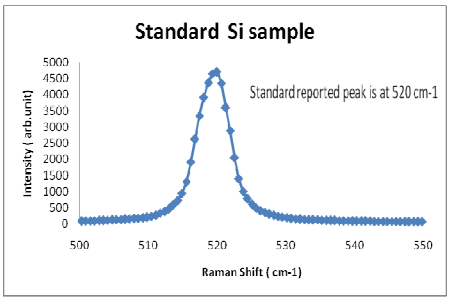

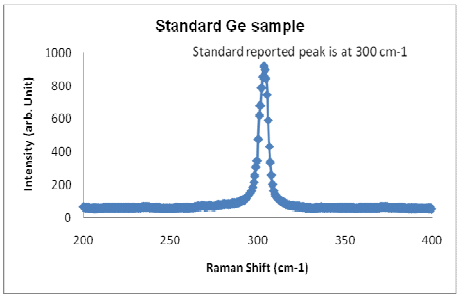

Fig.3. Raman Shift in cm^{-1} plotted with Intensity in arb. units for Si and Ge standard samples.

In the last five years or so, we have seen very rapid and significant developments in Raman scattering experiments on GaN and related nitride compounds [6]. In the GaN thin films, the Raman scattering study was performed in the back scattering $[Z(XY)\bar{Z}]$ geometry, where the z-axis is directed along the wurtzite c-axis. The wurtzite GaN structure belongs to $C_{6v}^{4}(P6_3mc)$ space group with two formula units per primitive cell, having Raman active optical modes at the centre of the Brillouin zone

$$\Gamma = A_1(z,z^2,x^2+y^2) + 2B_1 + E_1(x,y,xz,yz) + 2E_2(x^2-y^2,xy)$$

.

The B_1 modes are silent in Raman scattering where A_1 and E_1 modes are polar and hence, exhibit different frequencies for the transverse-optical (TO) and longitudinal-optical (LO) phonons, because of the macroscopic electric field associated with the LO phonons. The non-polar E_2 modes have two frequencies, namely, E_2 (high) and E_2 (low) associated with the motion of nitrogen (N) atoms and gallium (Ga) sub-lattice, respectively [**R**]. However, in the back scattering geometry of highly c-axis oriented GaN, only A_1 (LO) and E_2 modes are allowed, but we observe most of the Raman active modes in the PLD grown GaN films, confirming the polycrystalline as well as multiple orientation of the films. The comparison of observed phonon frequencies with the theoretical values of wurtzite GaN is shown in Table I.

TABLE I
Phonon modes in wurtzite GaN

Symmetry	Active in	Present Experiment (cm^{-1})	Theory (cm^{-1})
E2 (low)	Raman		146
A1(TO)	Raman, IR	533	534
E1(TO)	Raman, IR	561	556
E2 high	Raman	569	560
A1(LO)	Raman, IR	735	735
E1(LO)	Raman, IR	740	743
B1(low)	(silent)		335
B1 (high)	(silent)		697

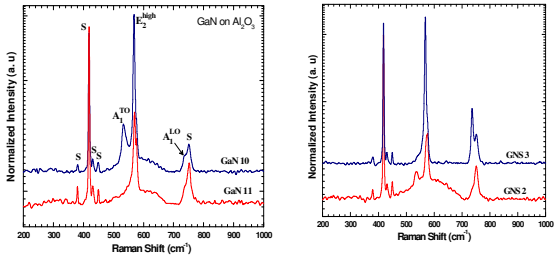

Fig. 4. Raman Spectra of GaN at different growth temperatures: 300°C- 600 °C

Fig.4 clearly shows that all the expected peaks are present. Peaks identified as 'S' are the Raman active peaks coming from the Al_2O_3 substrate. On comparison of four spectra, it is clear that at the higher deposition temperature the crystalline quality and the c-axis orientation were improved. It is shown from the spectra labeled GaN10 and GaN11, that the modes A_1(TO) and A_1(LO) along with the E_2 (high) are present in sample GaN10, however, the A1(TO) is missing in sample GaN11 grown at higher temperature. Thus, as the temperature increases the crystalline nature of the GaN or the nucleation layer increases. Usually, hexagonal phase is dominant in the mixed cubic-hexagonal nucleation layer. Thus, these Raman results indicate the presence of strong hexagonal modes for GaN nucleation layers. Intuitively, it is also clear that frequencies are shifted with respect to the corresponding A_1 and E_2 phonon modes in hexagonal GaN. The decrease in mode frequency implies the presence of in-plane tensile strain in these GaN nucleation layers. The results are now widely used to characterize carrier-transport properties, low-dimensional structures of nitrides such as quantum dots and superlattices etc.

B) Cu_2ZnSnS_4 (CZTS)

Cu_2ZnSnS_4 (CZTS) and $Cu_2ZnSnSe_4$ (CZTSe) based solar cells are promising candidates for low cost solar cells due to the natural abundance and low toxicity of the constituent elements [7]. CZTS crystallizes in three different states:

i) kesterite (KS; space group I_4 ; no. 82),
ii) stannite (ST; space group I_42m; no. 121),
iii) or primitive mixed Cu-Au (PMCA; space group P_42m; no. 111)

Crystal structures: KS and ST structures are body-centered tetragonal with c_2a (e.g., pseudocubic) symmetry and may be thought of as two sulfur face-centered cubic (FCC) lattices stacked on top of each other with Cu, Zn, and Sn occupying half the tetrahedral voids within this FCC lattice. The PMCA structure is primitive tetragonal with c _ a; two unit cells.

Phonons at the Γ point are classified according to the irreducible representations of the point group. For the KS structure, $\Gamma = 3A + 6B + 6E_1 + 6E_2$. Amongst these modes, A, B, E_1, and E_2 modes are Raman active and B, E_1, and E_2 modes are IR active. For the ST structure, $\Gamma = 2A_1 + A_2 + 2B_1 + 4B_2 + 6E$, and amongst these modes, A_1, B_1, B_2, and E vibrational modes are Raman active and B_2 and E modes are IR active. While the PMCA structure gives $\Gamma = 2A_1 + 2A_2 + B_1 + 4B_2 + 6E$. Amongst these modes, A_1, B_1, B_2, and E modes are Raman active, whereas 10 B_2 and E modes are IR active. The KS structure is the most stable amongst the three structures, albeit by only 5 meV/atom.

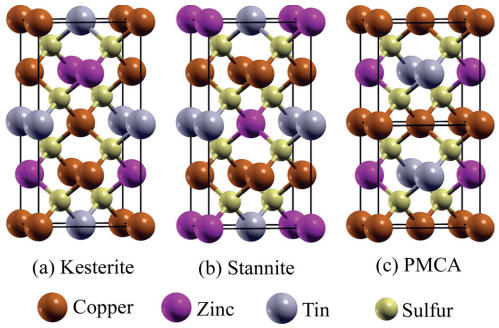

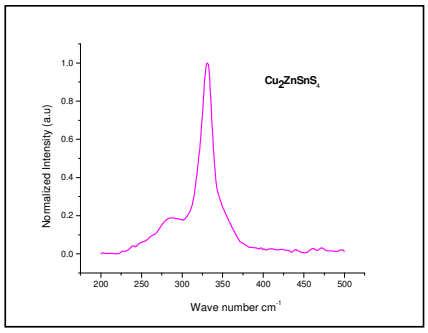

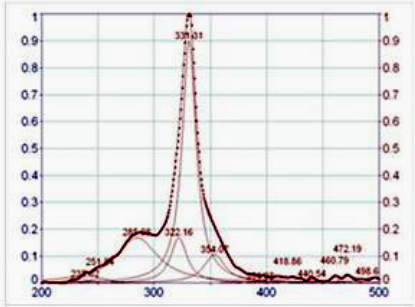

Figure 5 Structure and spectra of CZTS

TABLE II
Phonon modes in KS structure in CZTS

Symmetry	Active in	Present Experiment (cm^{-1})	Theory(cm^{-1})
A	Raman	331	340
A	Raman,	282	284
A	Raman,		272
B(TO)	Raman	351	355
B(LO)	Raman,		374
E(TO)	Raman,	351	351
E(LO)			366

The most intense Raman peak from CZTS films has been observed around 331 cm^{-1} and varies with the synthesis method though reports of 337–338 cm^{-1} are the most common. The most frequently observed 331 cm^{-1} peak is closest to the calculated A mode of the 340 cm^{-1} CZTS KS structure.

C) Doped Lithium Niobate ($LiNbO_3$)

Ferroelectric $LiNbO_3$ is widely used in integrated and guided-wave optics because of its favorable optical, piezoelectric, electro-optic, elastic, photo-elastic, and photorefractive properties [8]. $LiNbO_3$ has space-group R3c and has distorted perovskite type structure. Planes of oxygen atoms are arranged in a distorted hcp arrangement, with interstices alternatively filled bi Li, Nb atoms and vacancies. In a perfect crystal, each Li and Nb atom is surrounded by a distorted octahedron of O^{2+} ions. However, in a doped crystal the exact stoichiometry will vary depending on the growth process.
We have investigated the following doped samples :
1. **Mg-Ru** 4mol% Mg and 0.02 mol% Ru in $LNbO_3$
2. **Mg-Ru** 6mol% Mg and 0.02 mol% Ru in $LNbO_3$

Identification:
Ru- $LiNbO_3$ seed or Ru-L-N seed (wafer cut from the top portion of the as grown crystal of 0.022 mol% doped LN); **Ru- $LiNbO_3$bottom or Ru-L-N bottom** (wafer cut from the bottom portion of the as grown crystal of 0.022 mol% doped LN).

II. Method of preparation

Single crystals of Lithium niobate were grown by high temperature Czochralski method at its melting point at about 1252 ^oC by using solid state synthesized powder of Li_2Co_3 & Nb_2O_5.The primitive unit cell of $LiNbO_3$ contains ten atoms with two formula units. Phonons at the Γ point are classified according to the irreducible representations of the point group R3c as $\Gamma = 4A_1 + 5A_2 + 9E$. The E modes are doubly degenerate, thus 27 modes are observed. A_1 and E modes are Raman active and it is expected that 13 phonon peaks will be obtained. However, actual numbers of peak will be depending on the relative orientation of the crystal with respect to the polarization direction of the incident and scattered laser beam. In the pure and undoped sample, following Raman peaks have been reported : 153, 237, 332, 432, 581 and 872 cm^{-1} respectively.

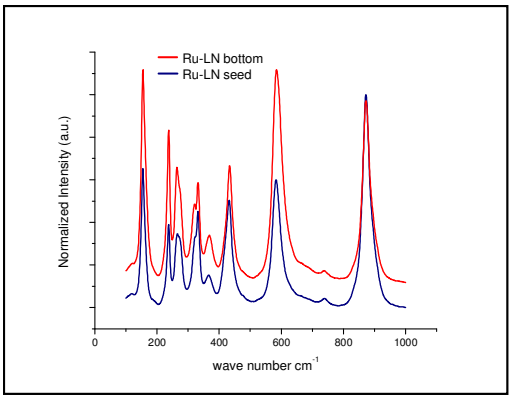

Figure 6 Raman spectra of doped lithium niobate

Using the curve fit soft ware, the deconvoluted peaks are:

Ru-L-N seed		Ru-L-N bottom	
Peaks (cm^{-1})	**Nature**	**Peaks (cm^{-1})**	**Nature**
117.8	small	119.3	small
153.8	sharp	154.1	sharp
237.2	sharp	237.2	sharp
265.05 and 272.2	Doublet	263.56 and 273.01	Doublet
323.2 and 331.7	Doublet	320.2 and 331.7	Doublet
366.0		368.0	
432.1		433.63	
583.3		584.8	
738.9		737.9	
872.7		872.7	

D) YVO_4: Eu^{+3}, Sm^{+3}

The Raman-active lattice vibrations of crystalline YVO_4:Eu^{+3},Sm^{+3} which crystallizes in the zircon-type structure in the tetragonal system, symmetries correspond to $I4_1/amd$ space group [9]. The unit cell contains two VO_4^{3-} anions and two Y^{3+} cations. Phonons at the Γ point are classified according to the irreducible representations of the point group as $\Gamma = 2A_{1g}+1A_{1u}+1A_{2g}+4A_{2u}+4B_{1g}+1B_{1u}+1B_{2g}+2B_{2u}+5E_g+5E_u$. The g-modes are Raman active and u-modes are IR-active. From group theory one can determine for the zircon type structure [10]:
Therefore, $\Gamma = 2A_{1g}+ 4B_{1g}+1B_{2g}+5E_g$

TABLE III
Phonon Raman modes in zircon type structure

D_{4h}	N	T_A	T	R	I	Polarization	Nature of modes
A_{1g}	2	0	0	0	2	$\alpha_{xx}+\alpha_{yy}, \alpha_{zz}$	Raman
A_{2g}	1	0	0	1	0		
B_{1g}	4	0	2	0	2	$\alpha_{xx}-\alpha_{yy}$	Raman
B_{2g}	1	0	0	0	1	α_{xy}	Raman
E_g	5	0	2	1	1	α_{xz}, α_{yz}	Raman

N-Total, T_A-Acoustics, T-Translation, R-Librational, I-Internal

It is clear that the maximum theoretically observable peaks are 12. Because of the equivalence of the axes X and Y for the tetragonal system, the geometrical configurations are X(ZZ)Y, X(YY)Z, (YX)Y, Z(YZ)X corresponding to the symmetry of the species A_{1g}, A_{1g}+ B_{1g}, B_{2g} and E_g, respectively. It is an inorganic nano phospher material having particle size between 20-30 nm. It is prepared by wet Chemical method

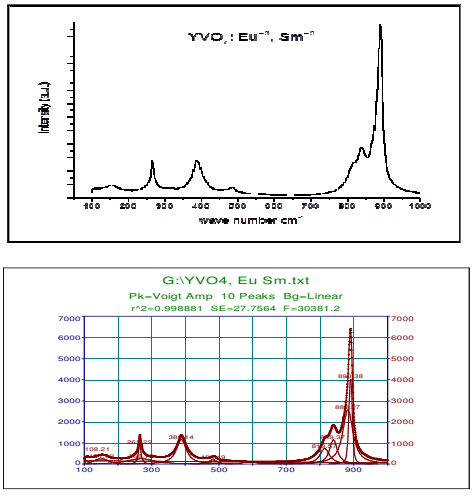

Fig.7. Raman spectrum and its deconvoluted peaks for YVO4:Eu^{+3},Sm^{+3}

TABLE IV
Phonon modes in YVO4:Eu^{+3},Sm^{+3}

Symmetry	Active in	Experiment (cm^{-1})	Theory(cm^{-1})
B_{1g}, Eg	Raman	151.8	156
B_{2g}	Raman	265.0	264
A_{1g}	Raman	389.1	380
B_{1g}	Raman	483.5	484
B_{1g}, Eg	Raman	818.5	817
	Raman	839.2	
A_{1g}	Raman	890.38	887
	Raman		913

E) Raman spectrum of Sb_2Te_3 under ambient conditions

The Raman-active lattice vibrations of crystalline Sb_2Te_3 whose symmetries correspond to the R3m space group (D^5_{3d}) with five atoms per unit cell were also investigated [11]. The crystal structure is rhombohedral and can be better visualized in the conventional hexagonal supercell with three formula units. The rhombohedral structure can be visualized as a layer structure and a hexagonal lattice cell. The hexagonal cell is formed by five individual atomic layers stacked along the *c* direction in the sequence Te–Sb–Te–Sb–Te, each layer containing a single atom in the unit cell. Phonons at the Γ point are classified according to the irreducible representations of the point group D^5_{3d} as
$\Gamma = 2(A_{1g} + E_g) + 3(E_u + A_{2u})$.

The g-modes (Raman active) and u-modes (IR-active).

TABLE V
Phonon modes in hexagonal Sb_2Te_3

Symmetry	Active in	Experiment (cm^{-1})	Theory(cm^{-1})
$E_g(1)$	Raman		49
$A_{1g}(1)$	Raman	67	69
$E_g(2)$	Raman	112	112
$A_{1g}(2)$	Raman	167	165

However, some Raman active modes due to Te have also been observed. These peaks are identified as occurring due to the un-reacted Te. The result for Sb_2Te_3 is compared to the predicted frequencies from the lattice dynamical model. The frequency shifts of the Raman-active modes in the mixed crystals show single-mode and two-mode behaviour, which is in agreement with simple models for the substitution of antimony atoms for tellurium.

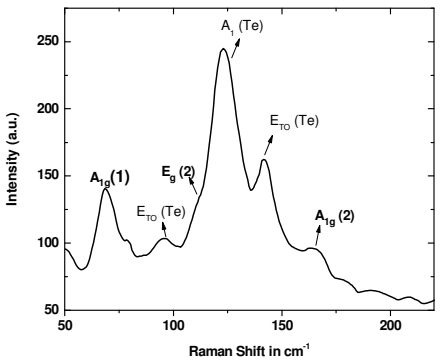

Fig. 8. Raman spectra of Sb_2Te_3 sample at ambient conditions

Figure 8 shows the Raman Spectrum obtained at 300K of the synthesized nanosized thermoelectric Sb_2Te_3 sample. We have observed three distinct modes at 69.04, 112, and 167.28cm^{-1} corresponding to the $A_{1g}(1)$, $E_g(2)$ and $A_{1g}(2)$ modes of Sb_2Te_3 respectively. Apart from these peaks which confirm the formation of Sb_2Te_3, prominent peaks occur at 96, 123 cm^{-1} and 141 cm^{-1}. These have been found to be associated with the presence of elemental Te in the sample and correspond to E_{TO}, A_1 and E_{TO} modes of Tellurium respectively. The occurrence of these peaks due to Te indicate that although Sb_2O_3 has been synthesized successfully, however the synthesis process may not have completed. Owing to large polarizability change associated with these vibrations, they have considerable intensity. The following table shows the peaks observed and their possible assignments.

TABLE VI
Assignments of the observed Raman modes for the sample under study

Observed peak (cm^{-1})	**Assignment**	**Phase**
69.04	$A_{1g}(1)$	Sb_2Te_3
79		
96	E_{TO}	Te
112	$E_g(2)$	Sb_2Te_3
123	A_1	Te
141	E_{TO}	Te
167.28	$A_{1g}(2)$	Sb_2Te_3

(2) Temperature dependent Raman Study:

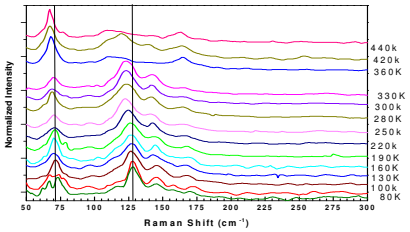

Fig. 9. Raman spectra of Sb_2Te_3 at various temperatures

Figure 9 shows the Raman spectra obtained for the sample at temperatures from 80 K to 440 K. At 80 K, we can readily observe that there are eight predominating peaks in the spectral range 50-175 cm^{-1}. These are found to be centred at 61, 67, 73, 117, 128, 145, 158 and 170 cm^{-1}. As mentioned earlier, the peaks observed at 128 and 145 cm^{-1} correspond to the A_1 and E_{TO} modes of the tellurium material. At 80K the low wave-number side shows additional peak at 61 cm^{-1} which is not observed at temperatures higher than 100 K. This may be the $E_g(1)$ mode of Sb_2Te_3 which has not been reported at ambient but is expected to occur around 50 cm^{-1} at room temperature.A few general trends can be inferred with increase in temperature. These include a general downshift in the observed wave-numbers for most of the observed modes. One can see from the figure that as we increase the temperature from 80k to 330k the number of peaks decreases along with intensity and there is increase in band width. In addition, at low temperatures, the observed peaks are sharp which subsequently broaden with increase in temperature. As a specific example, Figure 17 shows the FWHM vs Temperature graph from 80 K to 440K, for the band at158 cm^{-1} at 80 K which is $A_{1g}(2)$ mode of Sb_2Te_3. The figure also shows broadening with an increase in temperature in the A_1 mode of Te. With increase in temperature the peak position is shifted towards the lower frequency side. It is observed from the figure, that there is a sharp change at ~ 360K in both frequency and FWHM; in addition to this, the first order optical mode of Te almost disappears at this temperature. These two phenomena reveal a transition above 300K.At 300k in ambient temperature condition, we have observed three distinct modes at 69.04, 112, and 167.28cm^{-1} corresponding to the $A_{1g}(1)$, $E_g(2)$ and $A_{1g}(2)$ of Sb_2Te_3 respectively. And these three reported phonon modes move towards lower wave number side with increase in temperature. There is decrease in the number of peaks as well as intensity and for some peaks the band width increases and becomes wider from temperature region 360 to 440k corresponding to the observed phonon modes.Another interesting observation which can be made from the progression of Raman spectra is that as the temperature increases, although there is broadening and shifting of the peaks as discussed above, the modes occurring due to Tellurium which were prominent at 300K continuously broaden and lose intensity significantly and at the highest studied temperature of 440K, the predominant peaks are the ones occurring due to the various modes of Sb_2Te_3. All the three modes of Sb_2Te_3 at 440 K stand out as compared to the Te modes and are centred at 67.4, 108.5 and 163.4 cm^{-1} corresponding to the $A_{1g}(1)$, $E_g(2)$ and $A_{1g}(2)$ modes of Sb_2Te_3 respectively. This implies that with increase of temperature, the stoichiometry of the sample may be improving. It may be surmised that the annealing procedure for the sample preparation may need to be done at a higher temperature/longer duration.

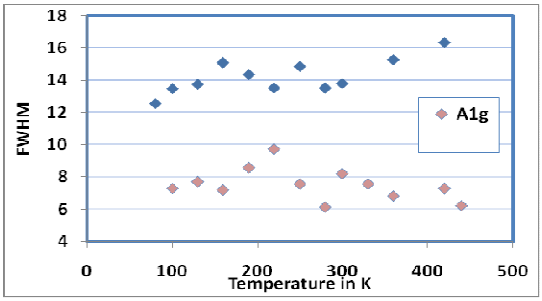

Fig. 10. Temperature dependent frequency and FWHM of $A_{1g}(2)$ mode.

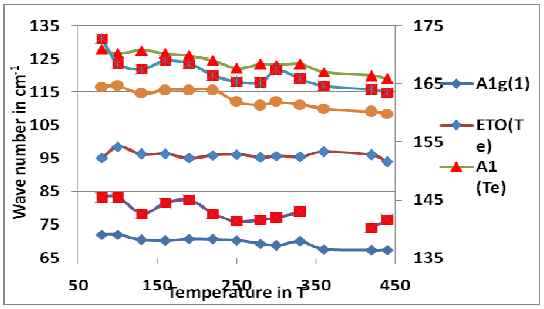

Fig. 11 Variation in frequency of the Raman modes with increase in temperature. The square markers correspond to the wave-numbers on the secondary axis on the right.

Acknowledgements

The authors are thankful to Prof. R.C. Budhani, Director, CSIR-NPL, New Delhi for his encouragement and support. As the samples are obtained from various groups, the authors are thankful to the scientists who have prepared and provided us for Raman Spectroscopic studies. Finally, the financial grant from the project fund NWP-45 (Advances in Metrology) is gratefully acknowledged.

References

[1]. A. K. Bandyopadhyay, Nita Dilawar, Arun Vijaya Kumar, Deepak Varandani and Dharambir Singh, *Bull. Mater. Sci. 21*, 433, 1998.

[2]. Sugandha Dogra, Nita Dilawar Sharma, Jasveer singh, Himanshu Kumar Poswal, S.M. Sharma and A.K. Bandyopadhyay, *High Pressure Research*, *Vol. 31*, No. 2, 292-303, June 2011.

[3]. Nita Dilawar ,Shalini Mehrotra, D. Varandani, B. V. Kumaraswamy, S. K. Haldar, A. K. Bandyopadhyay, *Materials Characterization 59*, 462-467, 2008.

[4]. Nita Dilawar, Deepak Varandani, Shalini Mehrotra, Himanshu Poswal, S.M. Sharma, A. K. Bandyopadhyay, *Nanotechnology 19,* 115703, 2008.

[5]. S. Mehrotra, A. K. Bandyopadhyay, *Journal of Alloys and Compounds 436*, 56-60, 2007.

[6]. V. N. Bessolov, Yu.V.Zhilyaev , E. V. Konenkova, V. A. Fedirko and D. R. T Zahn, *Semiconductors*, *37*, 940-943, 2003 and references there in.

[7]. Ankur Khare, Burak Himmetoglu, Melissa Johnson, David J. Norris, Matteo Cococcioni and Eray S. Aydil, *J. Appl. Phys*. *111*, 083707, 2012.

[8]. J. G. Scott, S. Mailis, C. L. Sones, R.W. Eason, *Appl. Phys. A 79,* 691–696, 2004.

[9]. G. Lu,C. Li, W. Wang, Z. Wang, H. Xia and P. Zhao, *Materials Science and Engineering*, *B 98*, 156-160, 2003.

[10]. Boriana Mihailova, *Crystallography*, 21-27, June, 2009.

[11]. G. C. Sosso1, S. Caravati and M. Bernasconi, *J. Phys.: Condens. Matter* 21, 095410-15, 2009.